Dark-field scattering microscopy for spectral characterization of polystyrene aggregates

Karsten Rebner,[1,3] Michael Schmitz,[2] Barbara Boldrini,[1] Alwin Kienle,[2] Dieter Oelkrug[3] and R. W. Kessler[1,*]

[1]*Department of Process Analytics, Reutlingen Research Institute, Alteburgstr. 150, D-72762 Reutlingen, Germany*
[2]*Institut für Lasertechnologien in der Medizin und Meßtechnik, Helmholtzstr. 12, D-89081, Ulm, Germany*
[3]*Institute of Physical and Theoretical Chemistry, University of Tübingen, Auf der Morgenstelle 8, D-72076 Tübingen, Germany*
**rudolf.kessler@reutlingen-university.de*

Abstract: Light scattering measurements of particle aggregates contain complex information which is difficult to decrypt. Dark-field scattering microscopy in the visible range is used to characterize multi-arranged polystyrene beads. First, measured light scattering spectra of single spheres are compared with the Mie theory. Then, additional spectral measurements of three different sample sets of sphere aggregates are carried out. The aggregates consist of homogeneous spheres and differ in number of spheres, arrangement and contact area. Principal component analysis is used to reduce the number of variables and achieve an accurate classification regarding the aggregate characteristics.

OCIS codes: (300.6550) Spectroscopy, visible; (290.5850) Scattering, particles; (010.1350) Backscattering; (290.4020) Mie theory; (100.5010) Pattern recognition

References and links

1. G. Mie, "Beiträge zur Optik trüber Medien, speziell kolloidaler Metallösungen," Ann. Phys. **330**(3), 377–445 (1908).
2. I. Itzkan, L. Qiu, H. Fang, M. M. Zaman, E. Vitkin, I. C. Ghiran, S. Salahuddin, M. Modell, C. Andersson, L. M. Kimerer, P. B. Cipolloni, K.-H. Lim, S. D. Freedman, I. Bigio, B. P. Sachs, E. B. Hanlon, and L. T. Perelman, "Confocal light absorption and scattering spectroscopic microscopy monitors organelles in live cells with no exogenous labels," Proc. Natl. Acad. Sci. U.S.A. **104**(44), 17255–17260 (2007).
3. H. Fang, L. Qiu, E. Vitkin, M. M. Zaman, C. Andersson, S. Salahuddin, L. M. Kimerer, P. B. Cipolloni, M. D. Modell, B. S. Turner, S. E. Keates, I. Bigio, I. Itzkan, S. D. Freedman, R. Bansil, E. B. Hanlon, and L. T. Perelman, "Confocal light absorption and scattering spectroscopic microscopy," Appl. Opt. **46**(10), 1760–1769 (2007).
4. Y. Liu, X. Li, Y. L. Kim, and V. Backman, "Elastic backscattering spectroscopic microscopy," Opt. Lett. **30**(18), 2445–2447 (2005).
5. M. I. Mishchenko, "Electromagnetic scattering by nonspherical particles: A tutorial review," J. Quant. Spectrosc. Radiat. Transf. **110**(11), 808–832 (2009).
6. T. Wriedt, "Light scattering theories and computer codes," J. Quant. Spectrosc. Radiat. Transf. **110**(11), 833–843 (2009).
7. J. D. Keener, K. J. Chalut, J. W. Pyhtila, and A. Wax, "Application of Mie theory to determine the structure of spheroidal scatterers in biological materials," Opt. Lett. **32**(10), 1326–1328 (2007).
8. K. Si, W. Gong, and C. J. R. Sheppard, "Model for light scattering in biological tissue and cells based on random rough nonspherical particles," Appl. Opt. **48**(6), 1153–1157 (2009).
9. R. Gupta, D. B. Vaidya, J. S. Bobbie, and P. Chylek, "Scattering properties and composition of cometary dust," Astrophys. Space Sci. **301**(1-4), 21–31 (2006).
10. H. Kimura, L. Kolokolova, and I. Mann, "Light scattering by cometary dust numerically simulated with aggregate particles consisting of identical spheres," Astron. Astrophys. **449**(3), 1243–1254 (2006).
11. F. J. Olmo, A. Quirantes, V. Lara, H. Lyamani, and L. Aladosarboledas, "Aerosol optical properties assessed by an inversion method using the solar principal plane for non-spherical particles," J. Quant. Spectrosc. Radiat. Transf. **109**(8), 1504–1516 (2008).
12. P. Yang, Q. Feng, G. Hong, G. Kattawar, W. Wiscombe, M. Mishchenko, O. Dubovik, I. Laszlo, and I. Sokolik, "Modeling of the scattering and radiative properties of nonspherical dust-like aerosols," J. Aerosol Sci. **38**(10), 995–1014 (2007).
13. L. X. Yu, R. A. Lionberger, A. S. Raw, R. D'Costa, H. Wu, and A. S. Hussain, "Applications of process analytical technology to crystallization processes," Adv. Drug Deliv. Rev. **56**(3), 349–369 (2004).

#119671 - $15.00 USD Received 9 Nov 2009; revised 11 Dec 2009; accepted 7 Jan 2010; published 28 Jan 2010

14. W. J. Cottrell, J. D. Wilson, and T. H. Foster, "Microscope enabling multimodality imaging, angle-resolved scattering, and scattering spectroscopy," Opt. Lett. **32**(16), 2348–2350 (2007).
15. Z. J. Smith, and A. J. Berger, "Construction of an integrated Raman- and angular-scattering microscope," Rev. Sci. Instrum. **80**(4), 044302 (2009).
16. T. A. Germer, "Light scattering by slightly nonspherical particles on surfaces," Opt. Lett. **27**(13), 1159–1161 (2002).
17. P. P. Banada, S. Guo, B. Bayraktar, E. Bae, B. Rajwa, J. P. Robinson, E. D. Hirleman, and A. K. Bhunia, "Optical forward-scattering for detection of Listeria monocytogenes and other Listeria species," Biosens. Bioelectron. **22**(8), 1664–1671 (2007).
18. S. Holler, S. Zomer, G. F. Crosta, Y. L. Pan, R. K. Chang, and J. R. Bottiger, "Multivariate analysis and classification of two-dimensional angular optical scattering patterns from aggregates," Appl. Opt. **43**(33), 6198–6206 (2004).
19. H. K. Roy, Y. Liu, R. K. Wali, Y. L. Kim, A. K. Kromine, M. J. Goldberg, and V. Backman, "Four-dimensional elastic light-scattering fingerprints as preneoplastic markers in the rat model of colon carcinogenesis," Gastroenterology **126**(4), 1071–1081, discussion 948 (2004).
20. F. Voit, J. Schäfer, and A. Kienle, "Light scattering by multiple spheres: comparison between Maxwell theory and radiative-transfer-theory calculations," Opt. Lett. **34**(17), 2593–2595 (2009).
21. C. F. Bohren, and D. R. Huffman, *Absorption and scattering of light by small particles* (Wiley-VHC, 1998).
22. A. D. Ward, M. Zhang, and O. Hunt, "Broadband Mie scattering from optically levitated aerosol droplets using a white LED," Opt. Express **16**(21), 16390–16403 (2008).
23. I. T. Jolliffe, *Principal Component Analysis* (Springer, 2002).
24. W. Kessler, Multivariate Datenanalyse für die Pharma-, Bio- und Prozessanalytik, 1 ed. (Wiley-VCH, 2006).
25. M. Schmitz, R. Michels, and A. Kienle, "Darkfield scattering spectroscopic microscopy evaluation using polystyrene beads," Proc. SPIE **7368**, 73681W (2009).
26. A. Curry, W. L. Hwang, and A. Wax, "Epi-illumination through the microscope objective applied to darkfield imaging and microspectroscopy of nanoparticle interaction with cells in culture," Opt. Express **14**(14), 6535–6542 (2006).
27. R. Michels, F. Foschum, and A. Kienle, "Optical properties of fat emulsions," Opt. Express **16**(8), 5907–5925 (2008).
28. S. N. Kasarova, N. Sultanova, C. Ivanov, and I. Nikolov, "Analysis of the dispersion of optical plastic materials," Opt. Mater. **29**(11), 1481–1490 (2007).
29. R. H. Boundy, and R. F. Boyer, *Styrene. Its polymers, copolymers and derivatives*. (Reinhold Publishing Corp., 1952).
30. X. Ma, J. Q. Lu, R. S. Brock, K. M. Jacobs, P. Yang, and X.-H. Hu, "Determination of complex refractive index of polystyrene microspheres from 370 to 1610 nm," Phys. Med. Biol. **48**(24), 4165–4172 (2003).
31. S. Tseng, A. Taflove, D. Maitland, V. Backman, and J. Walsh, "Extracting geometrical information of closely packed random media from multiply scattered light via a cross-correlation analysis," IEEE Antennas Wirel. Propag. Lett. **5**(1), 91–94 (2006).
32. K. Rebner, T. Merz, and R. W. Kessler, "Hyperspectral imaging — a novel concept for marker free chromosome characterization," in EMC 2008 14th European Microscopy Congress, Volume **3**: Life Science (2008), pp. 281–282.

1. Introduction

Over 100 years ago Gustav Mie [1] described the scattering of electromagnetic radiation by a homogeneous isotropic sphere; however, most particles do not follow these assumptions. Nevertheless single spheres can be regarded as the simplest model for any unknown shape. The technique of scattering spectroscopic microscopy enables the label-free determination of slight differences in refractive index or structure size [2–4]. The characterization of non-spherical particles or aggregates has become very important for various applications in science and industry. Theoretical and practical reviews [5,6] as well as studies in life science [7,8], astrophysics [9,10], remote sensing [11,12] and process analytics [13] reveal the diversity of non-spherical materials. Light scattering intensities are measured as not only spectral but also angular resolved patterns [14,15]. In most cases a comparison of minima and maxima positions of the scattered patterns is applied to define the particle properties. The scattering behavior of non-spherical particles, especially on substrates, can differ significantly from ideal Mie-scattering particles [16]. Complex matrix surroundings with changes in sphere shape or aggregation often result in scattering patterns which cannot be easily modeled.

For practical uses it is important to understand how the non-sphericity of particles influences the measured light scattering. Recent light scattering approaches involve multivariate data analysis (MVA) methods. One direction that has been taken is the use of explorative data structure modeling by using techniques such as principal component

#119671 - $15.00 USD Received 9 Nov 2009; revised 11 Dec 2009; accepted 7 Jan 2010; published 28 Jan 2010

analysis. The objectives of this technique are the visualization, classification and discrimination of light scattering patterns from large data sets [17]. Advanced light scattering methods combine different measuring techniques in which the multidimensional information is analyzed by MVA methods. The use of polar angle, θ, and azimuth angle, ϕ [18], in combination with wavelength, λ, and the polarization state [19] makes MVA analysis indispensable.

The aim of the present work is to show that dark-field scattering microscopy is able to characterize spheres and aggregates by means of their spectral light scattering behavior. In the first part of this work single particle measurements are compared with Mie calculations. Measurements of particle aggregates are described in the second part. The complexity of aggregate structures is due not only to the increased size, but also to the presence of contact areas between the particles and in spatial configurations that can be difficult to model. For such a system it is difficult to identify the plethora of information which is included in adequate theoretical models [20]. Nevertheless, an interpretation and characterization of the aggregated structures is made possible by means of MVA.

2. Theory

2.1 Single spheres: Mie theory

For evaluation of the scattering spectra of single spheres the Mie theory has to be adapted to the backscattering geometry of the experimental setup (Fig. 1). The single sphere is situated in the origin of the coordinate system. The polar coordinates θ and ϕ are suitable to describe the scattering. The incident light is regarded as a plane wave striking the optical axis (z-axis) in a cone with the angle α. Its intensity is given by $I_0(\lambda)$ measured with a spectrally flat reflectance standard placed at $z = 0$. Only backscattered light within the maximum angle of acceptance, β, is detected by the system. For a homogenous sphere and unpolarized light the differential scattering cross section is given by [21]

$$\frac{\mathrm{d}C_{\mathrm{sca}}(\lambda)}{\mathrm{d}\Omega} = \frac{S_{11}(\Theta,\lambda)}{k^2} \tag{1}$$

with the scattering cross section C_{sca}, the Stokes parameter S_{11} and the wavenumber k.

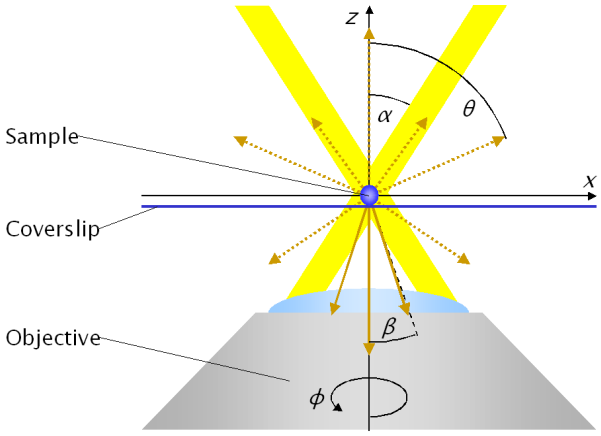

Fig. 1. Scheme describing the rotationally symmetric geometry of the setup. The sample is illuminated by a plane wave with an angle of incidence α. Only light that is scattered within the maximum angle β is detected by the setup (solid arrows), whereas the dashed arrows indicate non-detected light.

#119671 - $15.00 USD Received 9 Nov 2009; revised 11 Dec 2009; accepted 7 Jan 2010; published 28 Jan 2010

To obtain the measured spectrum, $I(\lambda)$, the differential scattering cross section has to be integrated over all detected scattering angles, $\Theta(\theta,\phi)$, which can be calculated by the incident ($\boldsymbol{k}_i$) and the scattered ($\boldsymbol{k}_s$) wave vectors

$$\Theta = \arccos \frac{\mathbf{k}_i \cdot \mathbf{k}_s}{|\mathbf{k}_i| \cdot |\mathbf{k}_s|} \text{ with } \frac{\mathbf{k}_i}{|\mathbf{k}_i|} = \begin{pmatrix} \sin\alpha \\ 0 \\ \cos\alpha \end{pmatrix} \text{ and } \frac{\mathbf{k}_s}{|\mathbf{k}_s|} = \begin{pmatrix} \sin\theta\cos\phi \\ \sin\theta\cos\phi \\ \cos\theta \end{pmatrix}. \quad (2)$$

Finally, the theoretical curve is convolved with a Gaussian function, $s(\lambda)$, considering the spectral resolution of the detector

$$\frac{I(\lambda)}{I_0(\lambda)} \propto \frac{1}{k^2} \int_{\theta=\pi}^{\pi+\beta} \int_{\phi=0}^{2\pi} S_{11}(\Theta(\theta,\phi,\alpha),\lambda) * s(\lambda) \sin\theta \, \mathrm{d}\theta \, \mathrm{d}\phi \, . \quad (3)$$

Equation (3) does not include any effects due to the coverslip. Ward et al. [22] showed this problem could be avoided by trapping aerosol droplets in the focus with the aid of optical tweezers.

2.2 Principal Component Analysis (PCA)

Multivariate Data Analysis (MVA) refers to a wide-ranging group of statistical techniques designed to evaluate the relationship among large multidimensional data sets. Principal Component Analysis (PCA) [23,24] plays a key role especially in the identification of significant experimental features when no a priori knowledge about the system under observation is available. PCA is a pure mathematical transformation that converts a number of correlated variables into uncorrelated variables called *principal components (PCs,* or *latent variable LVs)*. It consists of the decomposition of the experimental data matrix, $\boldsymbol{X}$, into smaller matrices:

$$\mathbf{X} = \mathbf{T}\mathbf{P}^{\mathbf{T}} + \mathbf{E} \quad (4)$$

where $\boldsymbol{T}$ and $\boldsymbol{P}$ are respectively the *score* and *loading* matrices obtained for the selected number of principal components and $\boldsymbol{E}$ is the residual matrix. The solution is unique and the principal components are uncorrelated and orthonormal. PCA scores are the orthogonal projection of the data samples on the axis of the new PC space. PCA loadings are the weights of each original variable in the calculation of the PCs. The first principal component (PC1) explains most of the total variance of the original data set. The second principal component (PC2) is orthogonal to the first and explains as much of the remaining variation as possible. Each newly extracted PC increases the amount of variance explained by the model until only random and experimental noise remains. Thereby, the first few PCs give an adequate description of the original data so that PCA can often be applied to reduce the dimensionality of a data set. Score plots and loading plots can then be employed for exploration and visualization of the data to recognize trends and relationship among samples and variables.

3. Materials and methods

3.1 Slide preparation

Two different types of spheres were used in the following experiments. The single sphere measurements were carried out with polystyrene beads with an average diameter of 2.8 µm. With the aid of an ultrasonic bath the beads were suspended in pure water. One droplet of this solution was air-dried on a quartz coverslip.

Certified monodisperse polystyrene particles with a diameter of 895 nm were used for the aggregate measurements. The particles were delivered as a 1% aqueous suspension and have a density of 1.05 g/cm^3 and a refraction index of 1.59 at 589 nm. Three different sample sets (s1, s2, s3) were prepared with a 0.1% working suspension. To minimize

#119671 - $15.00 USD Received 9 Nov 2009; revised 11 Dec 2009; accepted 7 Jan 2010; published 28 Jan 2010

particle coagulation, each working suspension was put in an ultrasonic bath. Quartz coverslips were used for each sample set. Small drops of the working suspension were then deposited on the slide. Afterwards, one slide (s1) was directly placed on the hot plate (40° C) for 10 min until all the water had evaporated. The two other slides (s2, s3) were air-dried for 60 min until all the water had also evaporated.

3.2 Experimental setup

Single and aggregate polystyrene measurements were performed with an optimized Microspectrometer of Zeiss MPM 800. The system is primarily aligned for mapping and imaging in the UV-VIS-NIR range. Unpolarized white light from a halogen lamp is coupled into a dark-field reflector and only peripheral beams of light are deflected to the standard dark-field objective (100x Zeiss LD Epiplan). The annular angle of illumination, α, is 65° and the maximum angle of detection, given by the numerical aperture NA = 0.75, β, is 48°. All backscattered light within the aperture is spectrally separated with a monochromator and detected by a photomultiplier in the image plane of the microscope. The spectral resolution of the system was described with a Gaussian function, $s(\lambda)$, having a standard deviation of 3.4 nm.

With a similar setup we have already measured the particles described in [25]. The darkfield illumination is realized with an axicon as described by Curry et al. [26].

3.3 Data processing

All spectra from each data set are analyzed using PCA to distinguish the different sphere characteristics. The spectra are pre-processed using first order derivative by Savitzky-Golay method (2nd polynomial, 5 smoothing points). Pre-processing and PCA have been performed using the Unscrambler 9.8 by Camo Software.

4. Results and discussion

4.1 Scattering pattern of single spheres

Figure 2 (a) and (b) show spectroscopic patterns of two different single polystyrene spheres '1' and '2' (dark blue). Both beads originated from the same suspension and were situated on the same coverslip. The scattered intensity is rather weak due to the fact that the particles are mainly forward scattering and only the backscattered light is observed. The theoretical curve (light green) was calculated with the described Mie theory and the sphere diameter, D, which was obtained by a correlation function $C(D)$ [see Eq. (5)]. In particular, the number and shape of the oscillations fit well to the theory. Basically, the spectra of both spheres seem to be equal; however, they are shifted and stretched against each other by a few nanometers in the wavelength. Assuming that both beads are spherical, homogenous and identical in their refractive indices, this difference must occur from diameter variations, which were also determined in bulk experiments with a collimated transmission setup [27]. The diameters of both spheres were identified by correlating the deviation of the measured curves with a set of theoretical curves, considering diameters from 0.5 µm to 5 µm (Fig. 2 (c))

$$C(D) = \sum_{\lambda} \frac{\mathrm{d}\left[\dfrac{I_{\mathrm{theory}}(\lambda, D)}{I_{0,\mathrm{theory}}(\lambda, D)}\right]}{\mathrm{d}\lambda} \frac{\mathrm{d}\left[\dfrac{I_{\mathrm{exp}}(\lambda)}{I_{0,\mathrm{exp}}(\lambda, D)}\right]}{\mathrm{d}\lambda} \,. \qquad (5)$$

The strongest correlation between theory and experiment can be found at the maximum of $C(D)$, in this case 2.785 µm and 2.807 µm respectively (see details in Fig. 2 (d)). Good match between theory and experiment is only possible with the correct optical properties of the sphere. The best correlation between theory and measured curves of all spheres could be obtained with the dispersion formula similar to that of Kasarova and Boundy [28,29] whereas with the dispersion relation of Ma [30] the results were slightly worse. Ma

#119671 - $15.00 USD Received 9 Nov 2009; revised 11 Dec 2009; accepted 7 Jan 2010; published 28 Jan 2010

measured the imaginary refractive index of polystyrene microspheres too. In the wavelength regime between 400 nm and 800 nm the imaginary part n_i is rather small (n_i < 0.0005), thus it is here neglected.

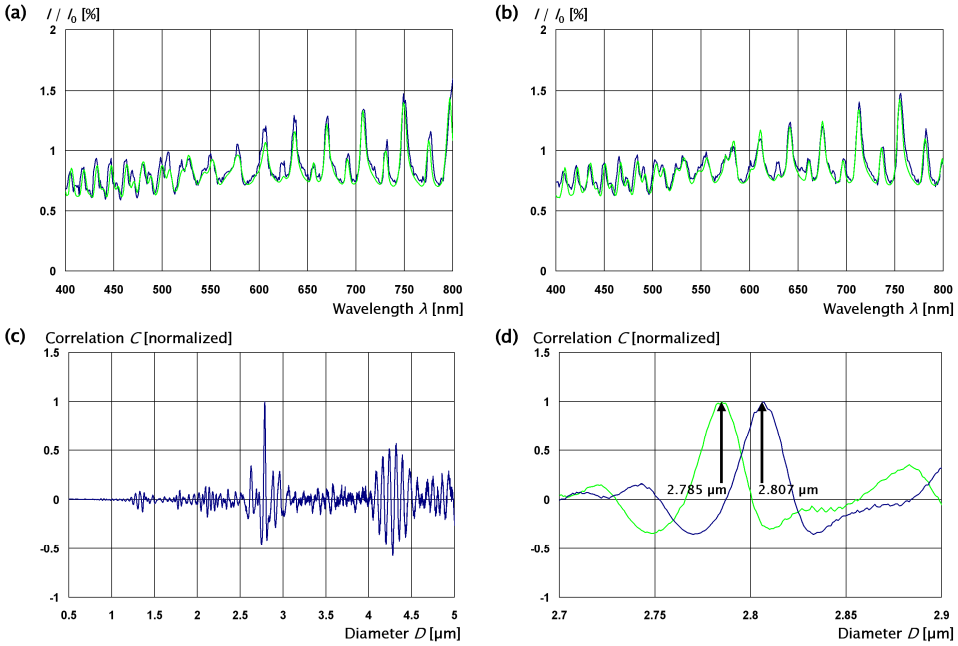

Fig. 2. (a)/(b) Experimental spectra (dark blue) I/I_0 of two different single polystyrene spheres '1'/'2' and theoretical (light green) spectra I/I_0 of a single sphere using the diameter obtained by the correlation function $C(D)$. (c) Correlation function $C(D)$ with the experimental data from single sphere '1'. (d) Detailed $C(D)$ of single sphere '1' (dark blue) and '2' (light green). The sphere diameters were determined via the maximum at 2.785 µm and 2.807 µm, respectively.

4.2 Scattering pattern of aggregates

A total number of twenty-four measurements from three different sample sets were carried out. Each set consisted of single spheres (895 nm) and highly ordered aggregates with an increasing number of uniformly spheres. According to the order of symmetry, the arrangement of the aggregates can be classified as linear (L) or non-linear (NL). Table 1 shows the labeling for each sample set.

Table 1. Labeling of each sample set and particle aggregate.

	Sample Set (s1)		**Sample Set (s2)**		**Sample Set (s3)**	
Number of spheres	**L**inear	**N**on-**L**inear	**L**inear	**N**on-**L**inear	**L**inear	**N**on-**L**inear
1	1_s1		1_s2		1_s3	
2	2_s1		2_s2		2_s3	
3	3L_s1	3NL_s1	3L_s2	3NL_s2	3L_s3	3NL_s3
4	4L_s1	4NL_s1	4L_s2	4NL_s2	4L_s3	4NL_s3
5	5L_s1	5NL_s1	5L_s2	5NL_s2	5L_s3	5NL_s3

Figure 3 (a) shows selected dark-field patterns of sample set s2. The measuring field, indicated as a dashed rectangle, had a fixed and equal size for all measurements and was placed in the middle of the field of view. Therefore, possible objective based aberration

#119671 - $15.00 USD Received 9 Nov 2009; revised 11 Dec 2009; accepted 7 Jan 2010; published 28 Jan 2010

effects or changed angular positions can be excluded. Sphere-substrate and sphere-sphere boundaries provide additional scattering effects from each aggregate.

This effect can be illustrated with normalized false color dark-field patterns, cf. Figure 3 (b). The yellow-red areas show high scattering effects due to interfaces of two or more spheres. The arrangements of s2 show point-shaped effects while s1 has more blurred areas. This behavior can be explained by the sample preparation. The faster water evaporation of s1 particles might lead to a closer sphere contact with slight deformations of the sphere. Changing these boundaries generate larger scattering domains.

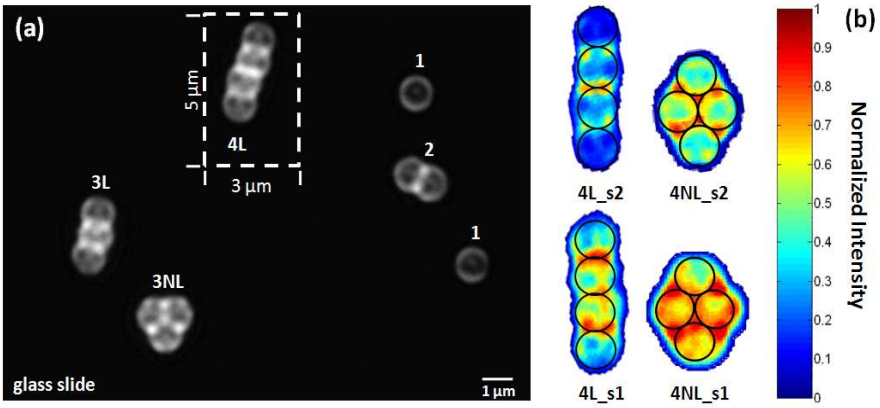

Fig. 3. Reflected dark-field image from a detailed section of sample set s2 (a). The arranged polystyrene spheres differ in sphere number and sphere geometry (L = linear; NL = non linear). (b) Normalized false color dark-field pattern from four arranged spheres of sample set s2 and s1.

Figure 4 shows the raw spectra of all sample sets together with their first order derivative. All reflection spectra show the same number of spectral bands and vary in spectral intensities and small wavelength shifts. The spectral information of a single sphere exists over all spectra and sample sets. Comparable results are reported by Tseng et al. Simulations [31] of closely packed cylinders show that the specific geometrical information of a single cylinder is still detectable, and the information level is not totally suppressed by the multi-scattering.

#119671 - $15.00 USD Received 9 Nov 2009; revised 11 Dec 2009; accepted 7 Jan 2010; published 28 Jan 2010

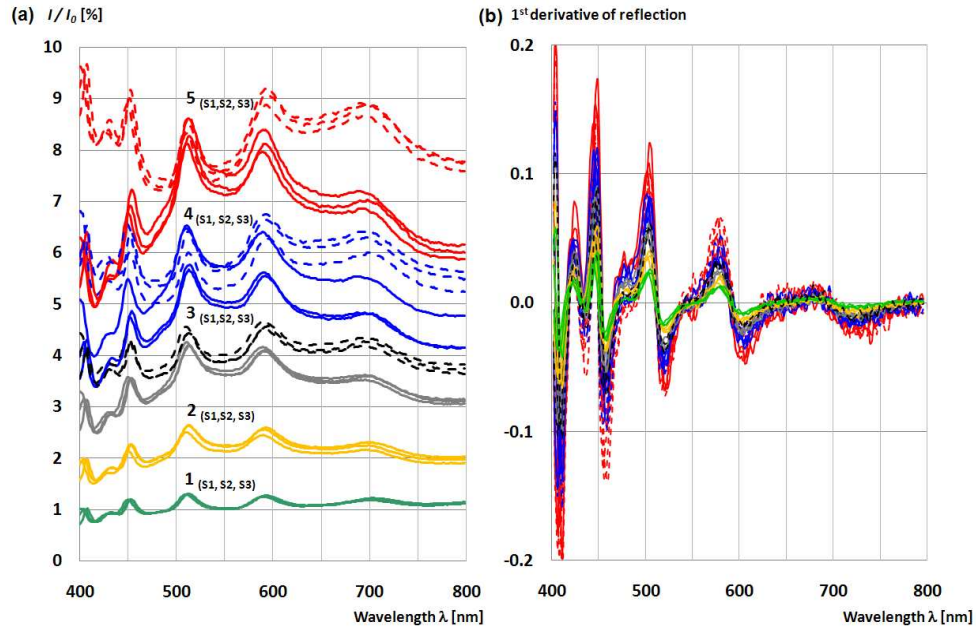

Fig. 4. (a) Reflection spectra for all sample sets and sphere arrangements (— linear;—non linear). (b) First order derivative spectra (Savitzky-Golay derivative, 5 points segment and 2nd order of polynomial).

Absolute light intensities over all wavelengths are slightly influenced by translations of the focus plane and increase non-linearly with increasing aggregate size. From a physical point of view, therefore the optical set up must kept constant. From the statistical point of view, this distortion of the physical background information can be extracted as long as the basic information is still present. Principal Component Analysis (PCA) analyses variations and is able to separate (orthogonal) the different superposed basic information. Thus it is possible to differentiate between the physics and the perturbation as could be shown in the next figures. Furthermore, the first order derivative of the acquired spectra improves the classification ability of the PCA. Derivative spectra are often employed in qualitative or quantitative spectroscopic analysis for background elimination, resolution enhancement, matrix suppression or discrimination between strong overlapping bands. In the present case the pre-processing suppresses the baseline offset and enhances the underlying spectral modulation. Small wavelength shifts become much more prominent with an improved spectral resolution.

4.3 Principal Component Analysis (PCA)

The first four PCs explain more than 97% of the entire variance and allow the characterization of the complete aggregate pattern. Higher PCs show mainly noise and the loadings represent no more specific particle characteristics. Figure 5 represents the score and loading plots of PC1 and PC2. The most distinguishable cluster partition in **PC1** represents the sample set s1, s2, and s3 which includes a small dependency of the number of particles, cf. Figure 5 (a).

#119671 - $15.00 USD Received 9 Nov 2009; revised 11 Dec 2009; accepted 7 Jan 2010; published 28 Jan 2010

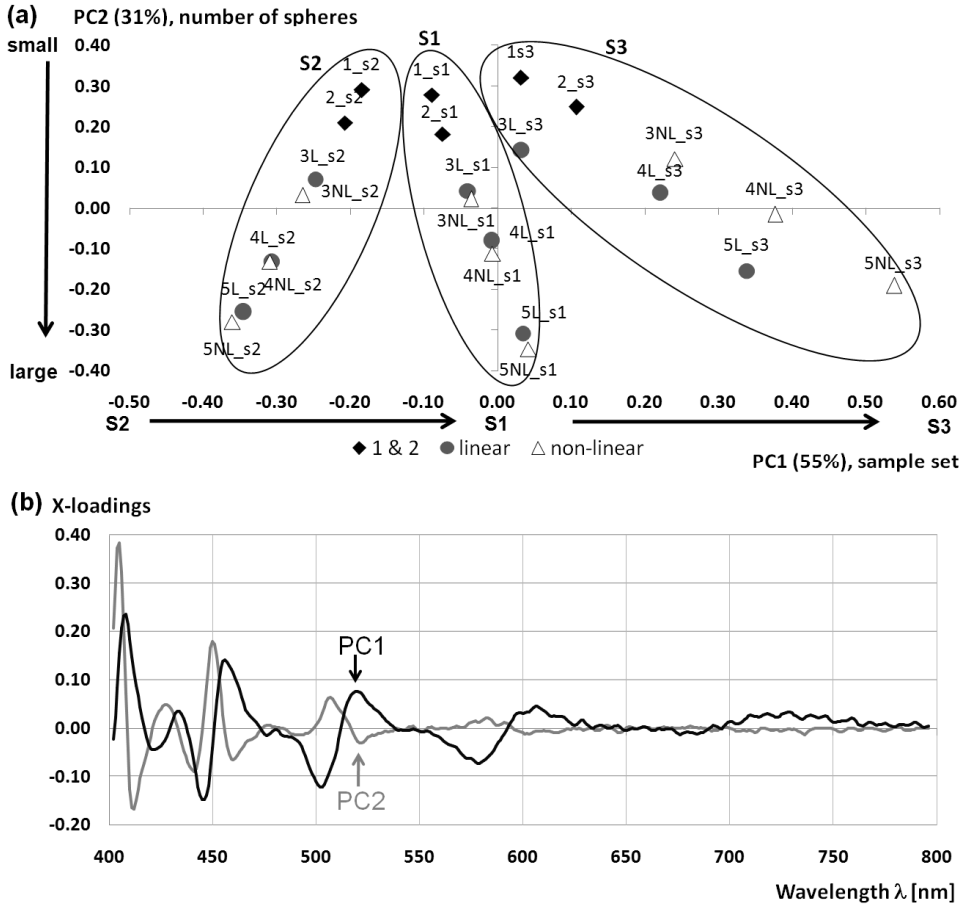

Fig. 5. Score (a) and loading (b) plots from PCA of first order derivative reflection spectra. The first two PCs explain 55% and 31% respectively of the total variance.

The first principal component can clearly separate the sample set s2 (with negative scores) and s3 (with positive scores), even though from the point of preparation there were no differences between these two sample sets. This result confirms the general difficulties in describing particle aggregates. While characteristic scattering effects of the aggregates are important, surrounding effects from the experimental setup and matrix effects from the sample itself also need to be taken into consideration. Small inequalities of the glass substrate or coupling effects cause small changes of the spectra between the sample sets. The first order derivative pre-processing identifies these small changes very clearly. Particles within a dried cluster bubble are closer together and therefore have a significant influence from this matrix effect. Particles which are outside of the main cluster can have a slightly different spectral signature. For a successful particle characterization it is important to suppress this unspecific information, while enhancing the particle's real characteristic.

The corresponding orthogonal **PC2** describes the number of spheres of all sample sets in a comparable way. High positive scores indicate small sphere arrangements whereas high negative scores specify higher arranged aggregates with influences of single and sphere- sphere interactions. The contact of a single sphere to another sphere results in a constant increase of additional scattering centers which can be visualized in PC2. Figure 5 (b) shows the corresponding loading plots for PC1 and PC2. Both PCs represent high spectral variances in the wavelength range from 400 nm to 600 nm. Here short wavelengths

#119671 - $15.00 USD Received 9 Nov 2009; revised 11 Dec 2009; accepted 7 Jan 2010; published 28 Jan 2010

are more important for the sample set and the number of spheres. Long wavelength ranges show only uncharacteristic small resonance effects of the particles.

Figure 6 (a) represents the aggregate characteristics. **PC3** separates clearly the sphere geometry in which linear aggregates have positive values while non-linear aggregates consequently have negative values.

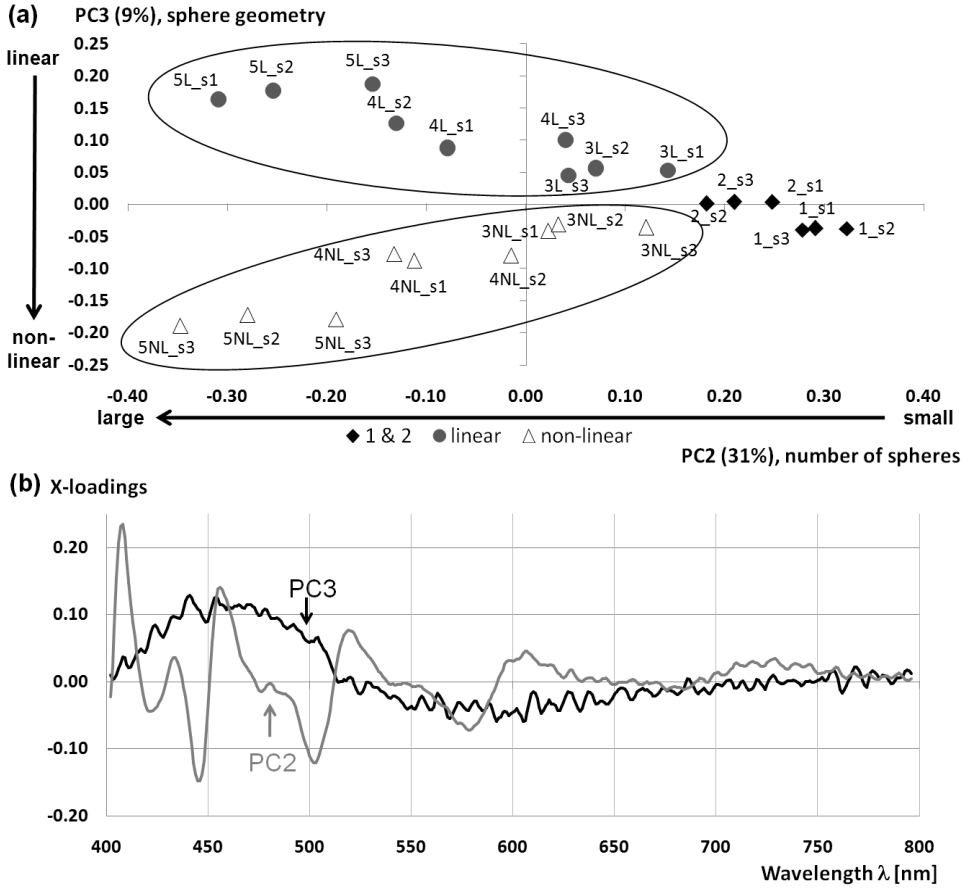

Fig. 6. Score (a) and loading (b) plots from PCA of the first order derivative reflection spectra. PC2 explain 31% and PC3 9% of the total variance.

With an increasing sphere number the geometry effect becomes more important for PC3. The differences in score values for the geometry increase strongly and can be explained by multiple particle-particle effects. An increasing sphere number combined with non-linear aggregations results in additional scattering centers. In Fig. 6 (b) the loading plot for PC3 indicates that smaller wavelengths (400-500 nm) are more prominent for linear aggregates (positive values). Wavelength intensities up to 500 nm are significant for non-linear geometry effects and indicate larger areas of scattering effects. Additionally, the loading for PC3 shows no specific spectral bands to characterize the geometry.

Figure 7 depicts the dependency of the particle geometry (PC3) and the modified scattering pattern of s1 (PC4). The differences of the score values in **PC4** are caused by the specific preparation step of sample set s1. Due to a faster water evaporation of s1, the aggregate formation seems to result in nanometer range size irregularities with more compressed aggregates. The small size irregularities are not detectable from the point of dark-field microscopy. However the nanometer sensitive interference pattern allows the

#119671 - $15.00 USD Received 9 Nov 2009; revised 11 Dec 2009; accepted 7 Jan 2010; published 28 Jan 2010

irregularities to be visualized and classified. The corresponding loading for PC4 has some specific band features which are more distinctive in the 400 – 600 nm range.

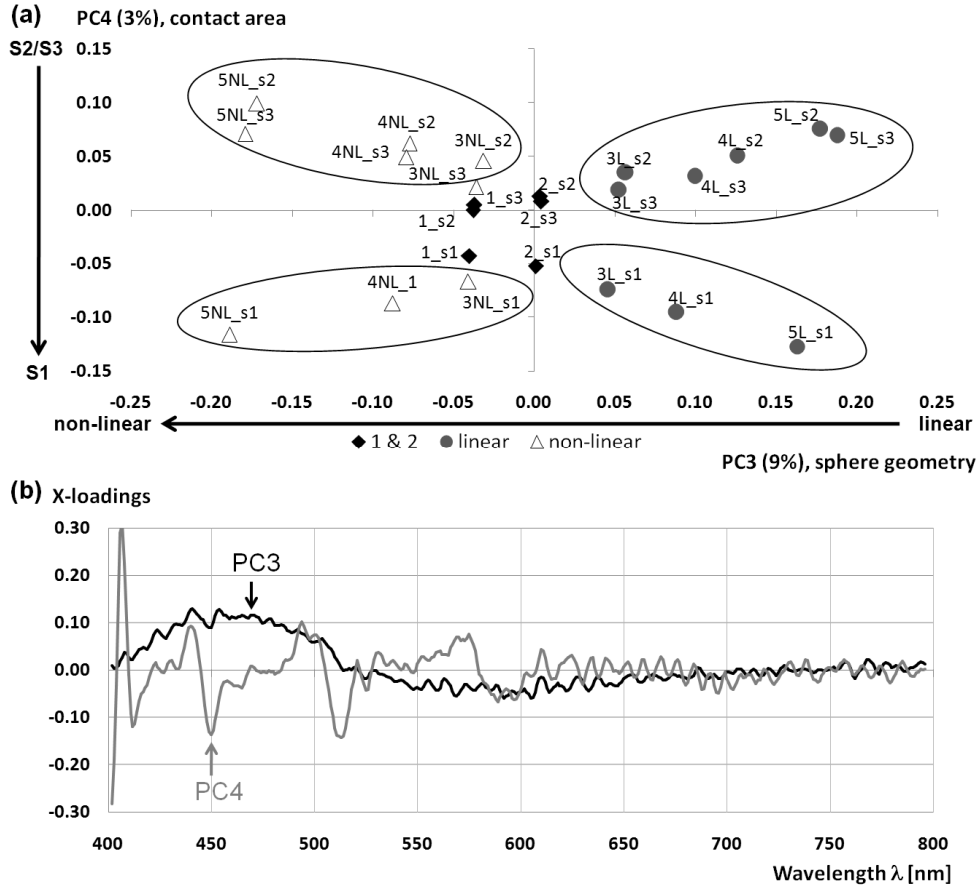

Fig. 7. Score (a) and loading (b) plots from PCA of the first order derivative reflection spectra. PC3 explain 9% and PC4 3% of the total variance.

5. Conclusion

In classical imaging microscopy a few nanometer difference in structure size is not observable, however, the presented results prove that they can be resolved with scattering spectroscopic microscopy. Therefore, it is e.g. possible to monitor temporal changes in size and refractive index which would not be possible with a classical light microscope due to the diffraction limit. In addition it is in principle possible to measure the dispersion functions of a material. Microscopic images can be used to illustrate the influence of boundaries in multi-sphere clusters. Due to the number of spheres, aggregate geometries and changes in contact area, the spectral information of such aggregates is, in comparison with single spheres, much more complicated. The PCA is able to separate these different contributions of sample characteristics and showed that matrix and substrate effects have an important influence on the spectral properties of spheres and aggregates. Therefore, in future work we want to investigate the interaction of particles on different substrates.

An existing application of the presented work is the classification of normal human metaphase chromosomes by backscattering spectroscopy in the visible range. In recent experiments [32] we could show that chromosome fine banding structures, similar to the boundaries of the sphere aggregates, lead to a sensitive chromosome characterization. In

#119671 - $15.00 USD Received 9 Nov 2009; revised 11 Dec 2009; accepted 7 Jan 2010; published 28 Jan 2010

comparison with particle aggregates of the same size, biological systems show smaller values of the relative refractive index and therefore less intense global scattering oscillations, as predicted by the Mie theory. The spectral smoothing is compensated by a larger complexity and diversification in size, shape and refractive index of the single scatterers forming the aggregate. In this case the spectra show underlying ripple structures with higher frequencies caused by different densely packed chromatin.

Acknowledgment

The work is supported by the Landesstiftung Baden-Württemberg Foundation under the contract "ZAFH Photon^{N}" and the Deutsche Forschungsgemeinschaft (DFG).

#119671 - $15.00 USD Received 9 Nov 2009; revised 11 Dec 2009; accepted 7 Jan 2010; published 28 Jan 2010